

## Probing the 2D to 3D Structural Transition in Gold Cluster Anions Using Argon Tagging

Wei Huang and Lai-Sheng Wang\*

*Department of Physics, Washington State University, 2710 University Drive, Richland, Washington 99354, USA*  
*Chemical & Materials Sciences Division, Pacific Northwest National Laboratory, MS K8-88,*

*P.O. Box 999, Richland, Washington 99352, USA*  
(Received 12 January 2009; published 15 April 2009)

Different physisorption properties by 2D and 3D isomers of  $\text{Au}_n^-$  clusters are observed and used to probe the 2D to 3D structural transition. Strong Ar clustering occurs on planar  $\text{Au}_n^-$  and the planar faces of the pyramidal  $\text{Au}_{20}^-$ . An abrupt change of Ar clustering at  $\text{Au}_{12}^-$  confirms the 2D to 3D structural transition at this size, where both isomers coexist. The minor 2D isomer can be titrated out by Ar to produce a clean 3D- $\text{Au}_{12}^-$  beam and beams of  $\text{Au}_{12}\text{Ar}_m^-$  with enhanced 2D isomers. Using the Ar titration and tagging, isomer-specific photoelectron spectra for the 2D and 3D  $\text{Au}_{12}^-$  are obtained.

DOI: [10.1103/PhysRevLett.102.153401](https://doi.org/10.1103/PhysRevLett.102.153401)

PACS numbers: 36.40.Mr, 61.46.Bc

Size-selected gold clusters have attracted significant attention since the discovery of unexpected catalytic effects by supported gold nanoparticles [1]. An interesting early finding in the study of size-selected  $\text{Au}_n^-$  clusters is the discovery of two-dimensional (2D) structures using ion mobility and density functional theory (DFT) calculations [2]. The planar gold cluster anions  $\text{Au}_n^-$  have been understood by the relativistic effects of gold [3,4] and confirmed by several subsequent experiments [5–7]. However, the critical size for the 2D to 3D structural transition has been controversial. Although the initial ion-mobility experiment showed that  $\text{Au}_{12}^-$  is the crossover size [2], DFT calculations continued to predict that 2D  $\text{Au}_n^-$  clusters are more stable than 3D isomers for much larger cluster size [5,8,9]. A recent study combining trapped ion electron diffraction and state-of-the-art electronic structure calculations has reaffirmed that the 2D to 3D transition does occur at  $\text{Au}_{12}^-$  [10]. This work further showed that DFT methods using traditional generalized gradient functionals are biased in favor of 2D structures and suggested that density functionals yielding accurate jellium surface energies are more suitable for gold clusters. By using the appropriate density functionals and including spin-orbit effects, zero-point energy correction, and thermal correction at 100 K, the authors showed that the 2D  $\text{Au}_{12}^-$  is 0.190 eV higher in energy than the global minimum 3D structure [10]. This result agrees well with both ion mobility [2] and photoelectron spectroscopy (PES) [5] experiments, which show that the intensity of the 3D isomer is about 2–3 times more intense than the 2D isomer; i.e., the 3D isomer should be slightly more stable than the 2D isomer for  $\text{Au}_{12}^-$ .

Model studies have shown that low dimensionality may be important for supported gold catalysts [11,12]. High-resolution electron microscopy has also revealed that very small gold clusters containing one or two atomic layers are the active species for catalysis [13,14]. Thus, understanding the properties of the size-selected 2D gold clusters and the 2D to 3D structural transition is of critical importance

in using gas-phase clusters as model systems to provide insight into the mechanisms of the catalytic effects of supported gold nanoparticles. Here we use argon tagging to probe the 2D to 3D transitions in negatively charged gold clusters. Weakly bound rare gas complexes have been widely used for action spectroscopy in cluster science [15,16]. They have also been used to provide structural information because different isomers may have different strengths of van der Waals interactions with rare gases [17,18]. In particular, in a previous study of the electronic photodissociation spectroscopy of  $\text{Au}_n^- \text{Xe}$  ( $n = 7–11$ ), planar gold clusters in the size range of 5–11, as well as  $\text{Au}_{20}^-$ , exhibit higher propensity for Xe physisorption [6], but argon complexes were not observed due to the more weakly bound nature between Ar and  $\text{Au}_n^-$ . In the current Letter, we report observation of extensive argon clustering onto planar gold clusters in the size range of  $n = 6–11$  and  $\text{Au}_{20}^-$ , which consists of four Au(111) faces [19]. The abrupt drop of argon clustering at  $\text{Au}_{12}^-$  provides clear evidence for the 2D to 3D transition. More interestingly, we find that the strong propensity of Ar physisorption onto planar clusters allows the planar isomer to be titrated out of the beam in the case of  $\text{Au}_{12}^-$ , for which both 3D and 2D isomers coexist, to produce a nearly clean 3D beam of  $\text{Au}_{12}^-$ , whereas the  $\text{Au}_{12}\text{Ar}_m^-$  beam contains enhanced populations of the 2D isomer. Using the Ar titration and tagging, we have been able to obtain isomer-specific PES spectra for  $\text{Au}_{12}^-$  for the first time.

The experiment was carried out using a laser vaporization supersonic cluster source equipped with a magnetic-bottle PES analyzer [20]. A gold disk target was vaporized by a pulsed laser to generate a plasma inside a cluster nozzle. A high-pressure helium (or He/Ar mixed) carrier gas pulse was delivered to the nozzle simultaneously to cool the plasma and help cluster growth. Clusters formed inside the nozzle were entrained in the carrier gas and underwent a supersonic expansion. Negatively charged clusters from the beam were extracted at  $90^\circ$  into a time-of-flight mass spectrometer. A PES experiment at 193 nm

(6.424 eV) was performed for selected cluster anions using the magnetic-bottle analyzer. The photoelectron kinetic energies were calibrated by the known spectra of  $\text{Au}^-$  and subtracted from the photon energies to obtain the reported electron binding energy spectra. The electron kinetic energy ( $E_k$ ) resolution of our apparatus is  $\Delta E_k/E_k \sim 2.5\%$ , i.e.,  $\sim 25$  meV for 1 eV electrons.

We intended to produce cold  $\text{Au}_n^-$  clusters by using a 10% Ar seeded helium carrier gas but found that under this condition extensive Ar clustering was taking place. The resulting  $\text{Au}_n\text{Ar}_m^-$  cluster distribution was very complicated due to the near mass degeneracy between five Ar atoms (200 amu) and one Au atom (197 amu). Subsequently, we diluted the 10% Ar carrier gas to about 1%–3% Ar by mixing in a pure helium stream using a needle valve. The resulting  $\text{Au}_n\text{Ar}_m^-$  cluster distribution is shown in Fig. 1 in the size range of  $n = 6$ –30. Because of the perpendicular cluster extraction in our mass spectrometer, only a limited range of clusters can be detected for a given deflector voltage used to compensate the transverse beam velocity. The overall bell-shaped distribution in each mass spectrum reflected the transmission of our time-of-flight mass spectrometer. But the local intensity variations can be used to judge the relative cluster abundances. Significant Ar clustering was observed, in particular, for  $n = 8$ –11 and 20, where more than four Ar atoms are physisorbed onto the gold clusters and the corresponding bare  $\text{Au}_n^-$  clusters become minor species.

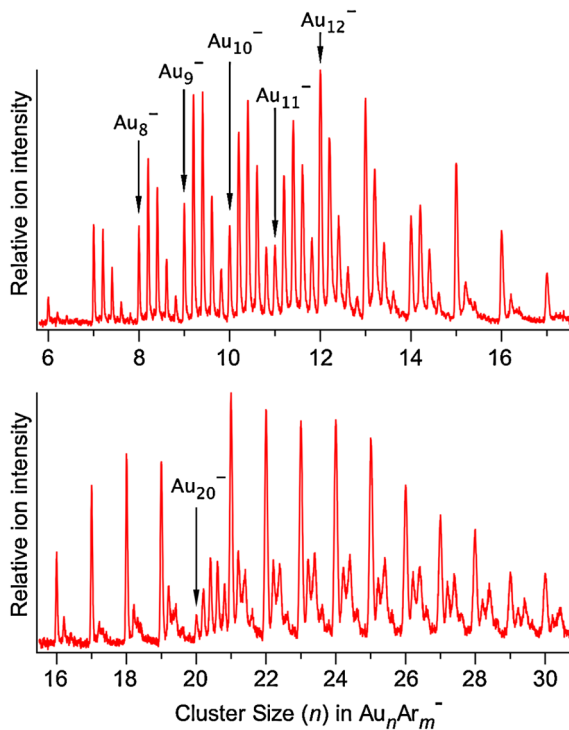


FIG. 1 (color online). Mass spectra of  $\text{Au}_n\text{Ar}_m^-$  produced from laser vaporization of a gold target with a helium carrier gas seeded with 1%–3% Ar. Note the extensive Ar clustering for  $\text{Au}_{7-11}^-$  and  $\text{Au}_{20}^-$  and the drop of Ar clustering at  $\text{Au}_{12}^-$ .

The size-dependent propensity for the physisorption of Ar to the  $\text{Au}_n^-$  clusters is striking; in particular, the extensive Ar clustering onto  $\text{Au}_{20}^-$  is quite dramatic in comparison to its neighbors. We should point out that a similar propensity for Xe clustering onto  $\text{Au}_n^-$  clusters has been observed previously [6], albeit in a less dramatic fashion. The enhanced ability for the formation of rare gas complexes by those  $\text{Au}_n^-$  clusters seems to be associated with their planarity. Although  $\text{Au}_{20}^-$  is a 3D cluster [19], its unique tetrahedral pyramidal structure consists of four Au(111) faces. The enhanced physisorption of the planar  $\text{Au}_n^-$  clusters can be understood by comparing the van der Waals interactions between a rare gas atom with a molecule and a planar surface [21]. The interaction potential of a rare gas atom with a molecule is proportional

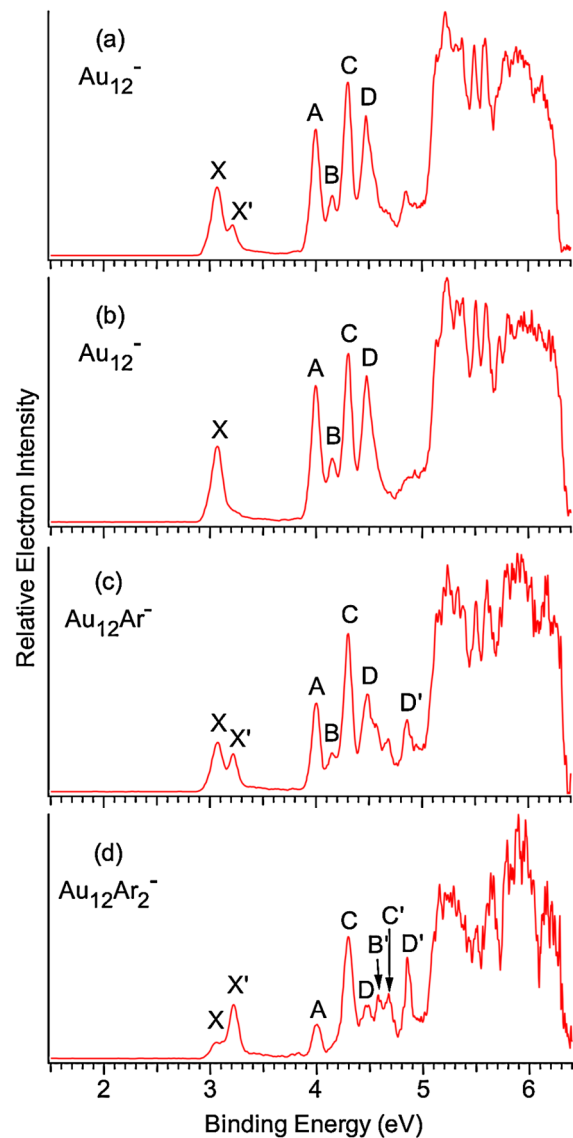


FIG. 2 (color online). The 193 nm photoelectron spectra of (a)  $\text{Au}_{12}^-$  using a pure He carrier gas, (b)  $\text{Au}_{12}^-$  using a He carrier gas seeded with 1%–3% Ar, (c)  $\text{Au}_{10}\text{Ar}^-$ , and (d)  $\text{Au}_{10}\text{Ar}_2^-$ .

to  $1/R^6$ , where  $R$  is the distance between the atom and the molecule. However, the van der Waals interaction between a rare gas atom with a surface is stronger and is proportional to  $1/R^3$  due to the pairwise additive nature between the interactions of the rare gas atom and the surface atoms [21]. Although the Au(111) faces in  $\text{Au}_{20}^-$  or the planar  $\text{Au}_n^-$  clusters are finite, one can readily understand that the interactions between Ar and a planar  $\text{Au}_n^-$  cluster are enhanced relative to a 3D isomer of the same size.

Definitive experimental evidence for the enhanced van der Waals interactions between Ar and planar  $\text{Au}_n^-$  clusters is provided by the photoelectron spectra of  $\text{Au}_{12}^-$  and  $\text{Au}_{12}\text{Ar}_m^-$  shown in Fig. 2. Figure 2(a) is a spectrum taken with a pure helium carrier gas, where the  $X$  and  $X'$  peaks correspond to the 3D and 2D isomers, respectively, as reported in detail previously [5]. The ratio of  $X/X'$  (i.e., 3D/2D) is about 2.3, which is similar to the previous ion-mobility data [2]. Figure 2(b) is a spectrum of  $\text{Au}_{12}^-$  taken with the 1%–3% Ar/He carrier gas, showing that the  $X'$  feature or the 2D isomer is almost completely gone. This observation suggests that the 2D  $\text{Au}_{12}^-$  has been titrated out of the  $\text{Au}_{12}^-$  beam by Ar, because of the enhanced interactions between Ar and the planar isomer. This is shown clearly in the spectra of the  $\text{Au}_{12}\text{Ar}_m^-$  complexes.

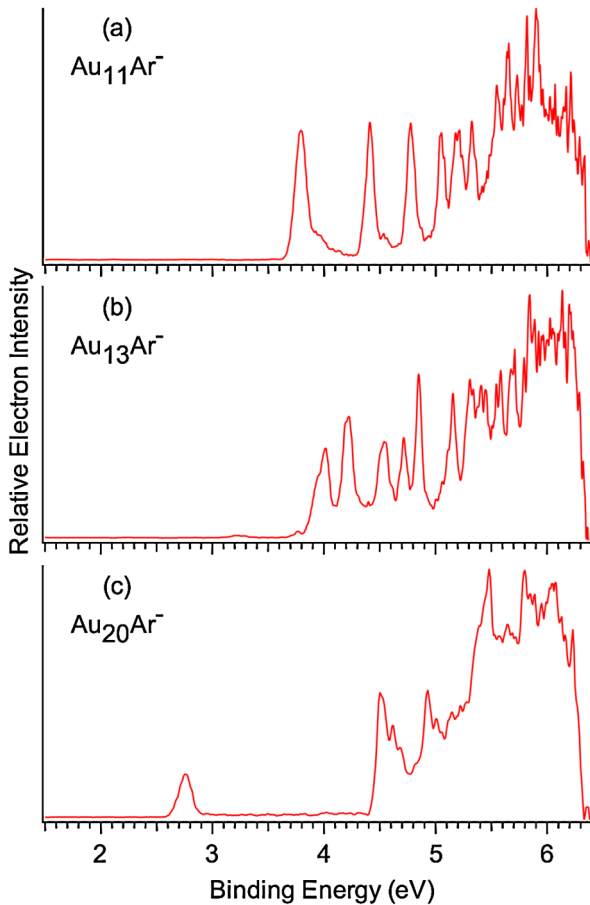


FIG. 3 (color online). The 193 nm photoelectron spectra of (a)  $\text{Au}_{11}\text{Ar}^-$ , (b)  $\text{Au}_{13}\text{Ar}^-$ , and (c)  $\text{Au}_{20}\text{Ar}^-$ .

The spectrum of  $\text{Au}_{12}\text{Ar}^-$  is similar to that of Fig. 2(a), except that the 2D contribution is significantly enhanced. Within our spectral resolution, the Ar complexation in  $\text{Au}_{12}\text{Ar}^-$  induced a negligible shift in the electron binding energies in the spectrum of  $\text{Au}_{12}\text{Ar}^-$  relative to that of the bare  $\text{Au}_{12}^-$ . The spectrum of  $\text{Au}_{12}\text{Ar}_2^-$  shows that the 2D isomer becomes the dominant species.

These observations imply that the interactions of Ar with 2D  $\text{Au}_n^-$  clusters are stronger than with 3D clusters, as revealed by the extensive Ar clustering for  $\text{Au}_{7-11}^-$  and  $\text{Au}_{20}^-$  (Fig. 1). These results also confirm unequivocally that  $\text{Au}_{12}^-$  is the crossover size from 2D to 3D structures and that the 3D- $\text{Au}_{12}^-$  is more stable than the 2D- $\text{Au}_{12}^-$ . However, the energy difference between the 3D and 2D  $\text{Au}_{12}^-$  must be very small because the physisorption of two Ar atoms reverses their stability; i.e., the 2D- $\text{Au}_{12}\text{Ar}_2^-$  is already more stable than the 3D- $\text{Au}_{12}\text{Ar}_2^-$ , as suggested by the relative intensities of the  $X$  and  $X'$  peaks in Fig. 2(d). Thus, our data show that even though the Ar complexation does not change the structures of the clusters, it can change the relative abundances of different isomers if their energies are very close. However, if energy separations between the 2D and 3D isomers are large, Ar complexation is expected to have little effect on the isomer distributions, as shown in Fig. 3, which shows that the spectra of  $\text{Au}_{11}\text{Ar}^-$ ,  $\text{Au}_{13}\text{Ar}^-$ , and  $\text{Au}_{20}\text{Ar}^-$  are identical to the bare clusters [5,19].

Figure 2 also allows isomer-dependent PES information to be obtained. In addition to the  $X'$  peak, new features  $B'$ ,  $C'$ , and  $D'$ , which become more clear in the  $\text{Au}_{12}\text{Ar}_m^-$

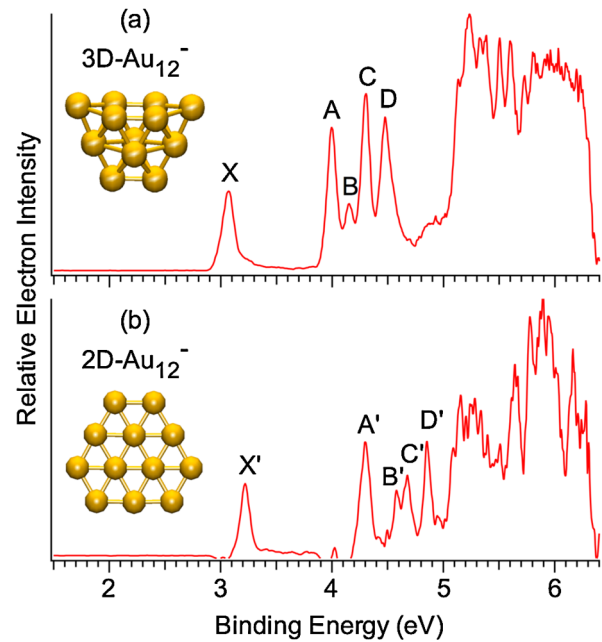


FIG. 4 (color online). Comparison of the isomer-specific photoelectron spectra of (a) 3D- $\text{Au}_{12}^-$  [the same as Fig. 2(b)] and (b) 2D- $\text{Au}_{12}^-$  obtained by subtracting (a) from Figs. 2(c) and 2(d). The insets show the 3D and 2D structures of  $\text{Au}_{12}^-$  from Ref. [5].

TABLE I. Measured vertical electron detachment energies for the low-lying transitions for the 3D and 2D isomers of  $\text{Au}_{12}^-$ . All energies are in eV, and the uncertainties are  $\pm 0.02$  eV.

3D- $\text{Au}_{12}^-$	2D- $\text{Au}_{12}^-$
3.06 (X)	3.22 (X')
3.99 (A)	4.30 (A')
4.15 (B)	4.58 (B')
4.30 (C)	4.68 (C')
4.47 (D)	4.85 (D')

spectra, should also be due to the 2D- $\text{Au}_{12}^-$  isomer. The peak C, which comes from the 3D- $\text{Au}_{12}^-$ , should contain contributions from the 2D isomer, because its relative intensity increases in the  $\text{Au}_{12}\text{Ar}_m^-$  spectra. Since the spectrum in Fig. 2(b) comes from a nearly pure 3D- $\text{Au}_{12}^-$  beam and because of the fact that there is a negligible binding energy shift between the spectra of the bare  $\text{Au}_{12}^-$  and the  $\text{Au}_{12}\text{Ar}_m^-$  van der Waals complexes, we can subtract the spectrum in Fig. 2(b) from the spectra of Figs. 2(a), 2(c), and 2(d) to obtain isomer-specific spectra for the 2D- $\text{Au}_{12}^-$ . The so-obtained spectrum for the 2D- $\text{Au}_{12}^-$  isomer is compared with the 3D- $\text{Au}_{12}^-$  spectrum in Fig. 4. Although the spectral subtraction is not perfect, the peak A', which overlapped with the peak C of the 3D isomer, is clearly resolved [Fig. 4(b)]. The high binding energy part of the spectra above 5 eV for both isomers is completely overlapped, and the spectral subtraction allowed the high binding energy features of the 2D isomer to be revealed quite clearly. The vertical electron binding energies for the labeled low-lying transitions in Fig. 4 are given in Table I for the two isomers. In addition to its higher electron binding energies, the 2D- $\text{Au}_{12}^-$  isomer also exhibits a larger energy gap of 1.08 eV (the X'-A' separation) relative to that of the 3D isomer (0.93 eV).

In conclusion, we observed extensive Ar clustering onto the planar  $\text{Au}_n^-$  clusters and the unique pyramidal  $\text{Au}_{20}^-$  cluster. This observation is understood on the basis of the strong physisorption of a surface relative to a molecule and is confirmed by the preferred Ar tagging onto the 2D- $\text{Au}_{12}^-$  over the 3D- $\text{Au}_{12}^-$  isomer. The Ar tagging also confirmed unequivocally that  $\text{Au}_{12}^-$  is the crossover size from 2D to 3D structures and that the two isomers of  $\text{Au}_{12}^-$  are very close in energy with the 3D isomer being slightly more stable. Isomer-specific photoelectron spectra were obtained for  $\text{Au}_{12}^-$  for the first time by using the Ar titration and tagging, which may also be used more generally for other clusters with close isomers [22] but very different structures.

We thank Professor Xiao Cheng Zeng and Professor Max Bertino for valuable discussions. This work was supported by the National Science Foundation (No. CHE-0749496) and performed at the W.R. Wiley Environmental Molecular Sciences Laboratory, a national

scientific user facility sponsored by DOE's Office of Biological and Environmental Research and located at Pacific Northwest National Laboratory, operated for DOE by Battelle.

\*[s.wang@pnl.gov

- [1] M. Haruta, *Catal. Today* **36**, 153 (1997); also see a recent thematic issue of *Chem. Soc. Rev.* **37**, 1759 (2008) for tutorial and critical reviews on related topics.
- [2] F. Furche, R. Ahlrichs, P. Weis, C. Jacob, S. Gilb, T. Bierweiler, and M.M. Kappes, *J. Chem. Phys.* **117**, 6982 (2002).
- [3] H. Hakkinen, M. Moseler, and U. Landman, *Phys. Rev. Lett.* **89**, 033401 (2002).
- [4] H.M. Lee, M. Ge, B.R. Sahu, P. Tarakeshwar, and K.S. Kim, *J. Phys. Chem. B* **107**, 9994 (2003).
- [5] H. Hakkinen, B. Yoon, U. Landman, X. Li, H.J. Zhai, and L.S. Wang, *J. Phys. Chem. A* **107**, 6168 (2003).
- [6] S. Gilb, K. Jacobsen, D. Schooss, F. Furche, R. Ahlrichs, and M.M. Kappes, *J. Chem. Phys.* **121**, 4619 (2004).
- [7] X.P. Xing, B. Yoon, U. Landman, and J.H. Parks, *Phys. Rev. B* **74**, 165423 (2006).
- [8] L. Xiao and L.C. Wang, *Chem. Phys. Lett.* **392**, 452 (2004).
- [9] P. Koskinen, H. Kakkinen, B. Huber, B. von Issendorff, and M. Moseler, *Phys. Rev. Lett.* **98**, 015701 (2007).
- [10] M.P. Johansson, A. Lechtken, D. Schooss, M.M. Kappes, and F. Furche, *Phys. Rev. A* **77**, 053202 (2008).
- [11] M. Chen and D.W. Goodman, *Acc. Chem. Res.* **39**, 739 (2006).
- [12] C. Zhang, B. Yoon, and U. Landman, *J. Am. Chem. Soc.* **129**, 2228 (2007).
- [13] S.N. Rashkeev, A.R. Lupini, S.H. Overbury, S.J. Pennycook, and S.T. Pantelides, *Phys. Rev. B* **76**, 035438 (2007).
- [14] A.A. Herzog, C.J. Kiely, A.F. Carley, P. Kandon, and G.J. Hutchings, *Science* **321**, 1331 (2008).
- [15] W.H. Robertson and M.A. Johnson, *Annu. Rev. Phys. Chem.* **54**, 173 (2003).
- [16] A. Fielicke, G. von Helden, and G. Meijer, *Eur. Phys. J. D* **34**, 83 (2005).
- [17] M.B. Knickelbein and W.J.C. Menezes, *J. Phys. Chem.* **96**, 6611 (1992).
- [18] E. Janssens, P. Gruene, G. Meijer, L. Woste, P. Lievens, and A. Fielicke, *Phys. Rev. Lett.* **99**, 063401 (2007).
- [19] J. Li, X. Li, H.J. Zhai, and L.S. Wang, *Science* **299**, 864 (2003).
- [20] L.S. Wang, H.S. Cheng, and J. Fan, *J. Chem. Phys.* **102**, 9480 (1995).
- [21] L.W. Bruch, M.W. Cole, and E. Zaremba, *Physical Adsorption: Forces and Phenomena* (Clarendon, Oxford, 1997).
- [22] An alternative technique for isomer-resolved photoelectron spectroscopy involves isomer selection using ion mobility, which has been demonstrated by R. Fromherz, G. Gantefore, and A.A. Shvartsburg, *Phys. Rev. Lett.* **89**, 083001 (2002).